Laser surface texturing of Wankel engine apex seals

PAPER • **OPEN ACCESS**

Laser surface texturing of Wankel engine apex seals

To cite this article: Nick Morris *et al* 2020 *Surf. Topogr.: Metrol. Prop.* **8** 034001

Surface Topography: Metrology and Properties

PAPER

Laser surface texturing of Wankel engine apex seals

Nick Morris[1], George Hart[1], Yong Jie Wong[1], Matt Simpson[1] and Sebastian Howell-Smith[2]

[1] Loughborough University, Leicestershire, United Kingdom
[2] Capricorn Automotive, Berkshire, United Kingdom

E-mail: N.J.Morris@lboro.ac.uk

Keywords: LST, laser surface texturing, texturing, friction, Wankel, rotary engine, apex seal

OPEN ACCESS

RECEIVED
7 May 2020

REVISED
15 July 2020

ACCEPTED FOR PUBLICATION
3 August 2020

PUBLISHED
10 August 2020

Abstract

Wankel rotary engines are used as power units in contemporary machines such as unmanned aerial vehicles and automobile range extenders due to their high-power density. A challenge of the engine architecture is the maintenance of an effective seal around each chamber while simultaneously minimising parasitic frictional losses. This paper investigates, experimentally, the suitability of laser surface texturing to reduce frictional losses at the apex seal-housing interfaces of Wankel engines. To inform the design of the laser surface texture features an analytical model is created to characterise the tribological properties of the apex seal-housing conjunction. The performance of the texture features is evaluated experimentally, and the results indicate that laser surface texture features can reduce frictional power loss by up to 30% at the apex seal-housing interface.

Nomenclature

A	Chamber Gas flow exchange or leakage area
A_b	Areas at the back of the seal
A_h	Section of housing areas swept during on crank degree
A_L	Apex seal Area exposed to leading cavity pressure
A_T	Apex seal Area exposed to Trailing cavity pressure
a_r	Radial Acceleration
a_t	Tangential Acceleration
b	Apex seal radial width between housing and rotor
b'	Apex seal radial width
C_d	Discharge coefficient
C_v	Specific Heat in constant volume
e	Scalar Shaft eccentric radius
E'	Reduced elastic modulus $\frac{2}{\frac{1-\nu_1^2}{E_1}+\frac{1-\nu_2^2}{E_2}}$
F_L	Reaction force of load cell
F_{pr}	Preload force
F_s	Leaf spring radial force
g_1	Viscous Non-Dimensional group
g_3	Elastic Non-Dimensional group
h	Central film thickness
G	Non dimensional parameter $\alpha_o E'$
k	Dimensionless trochoid constant $\left(\frac{\rho}{e}\right)$
l	Rotor width
m	Seal mass
$\dot{m}_i$	Time rate of change of Mass flow into chamber
$\dot{m}_o$	Time rate of change of Mass flow out of chamber
$\dot{P}$	Time rate of change of pressure in chamber
P	Chamber pressure
P_b	Pressure at the back of the seal
P_L	Pressure in leading cavity

P_T	Pressure in trailing cavity
r_x	Scalar component of housing shape in x direction
r_y	Scalar component of housing shape in y direction
R	Effective radius $\frac{1}{R_1^{-1}+R_2^{-1}}$
R_g	Gas constant
T	Chamber Temperature in chamber
T_a	Torque on housing of non apex seal contacts
T_i	Temperature of air into the chamber
T_F	Apex seal Friction toque on the housing
T_P	Torque on the housing created by chamber pressures
$\dot{T}$	Time rate of change of Temperature in chamber
U	Non dimensional parameter $\frac{\eta_0 \bar{U}}{E'R}$
$\bar{U}$	Entrainment velocity
V	Chamber Volume
$\dot{V}$	Time rate of change of chamber volume
V_m	Chamber Volume
w	Contact load per unit length
W	Dimensionless load $\frac{w}{E'R}$
W_h	Normal reaction force between the housing and the apex seal
W_r	Normal reaction force between the rotor and apex seal

Greek letters

α	Crank angle
α_o	Pressure viscosity coefficient
β	Rotor angle
γ	Ratio of the specific heats
ρ	Scalar Rotor generating radius
ρ_1	Density of air in enviroment
η_0	Lubricant viscosity at conjunctional inlet temperature
μ_h	Friction coefficient between the housing and apex seal
μ_r	Friction coefficient between the rotor and apex seal
ω_c	Crank shaft angular velocity
ω_r	Rotor angular velocity
λ	Oil film ratio parameter
σ_1	Apex seal RMS surface roughness
σ_2	Housing RMS surface roughness
φ_n	Normal direction to the surface areas A_h
φ	Angle of housing surface exposed to chamber pressure

Introduction

The parasitic frictional losses at the apex seal-housing interface of a Wankel rotary engine significantly affect overall efficiency, fuel consumption and CO_2 emission. For vehicular applications this would manifest as a reduction in range, specific fuel consumption and performance. It has been demonstrated by Yamamoto [1] that excessive friction generated by apex and side seals accounts for a 10% reduction in engine efficiency.

Zhang *et al* [2] report that the parasitic frictional loss for small Wankel engines can be in the region of ~10% of the engine output power. The authors showed that diamond like carbon (DLC) coatings can be used to reduce the friction torque. In addition to various surface coatings created for automotive applications [3], surface modification techniques such as laser surface texturing (LST) have become prominent during the preceding few decades as an effective approach to reduce frictional losses in a variety of contacts [4].

Laser surface texturing has been shown by Etsion and Sher [5] to reduce frictional losses by up to 5% at the piston ring-cylinder liner interface of automotive reciprocating internal combustion engines. Ryk *et al* [6] have shown that laser surface textured piston rings produce the greatest friction reductions at mid-stroke. Vladescu *et al* [7] showed that texturing placed on the stationary surface at mid-stroke (high entrainment velocity) of the piston reciprocating motion can reduce frictional losses by up to 50% at this location. In addition, it was shown textures at reversal (low entrainment speeds) have negligible effect on frictional losses and in some instances can worsen the

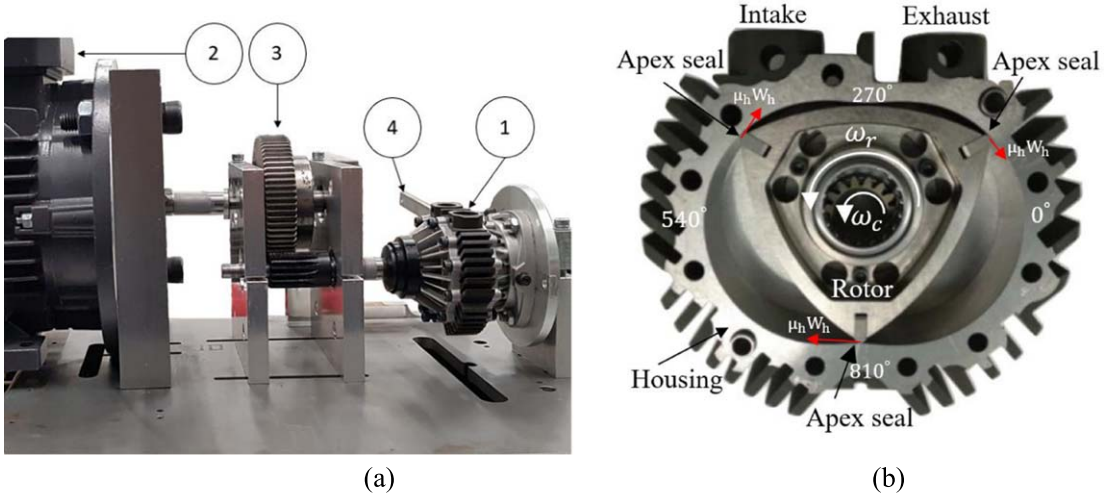

Figure 1. Test rig and engine.

losses incurred. A similar result for ring reversal was shown in a numerical analysis by Morris *et al* [8].

In recent years, the interaction of surface wear and friction of textured counter-formal tribological conjunctions has become of interest. Kovalchenko *et al* [9] showed that friction reduction in conformal and counter-formal conjunctions takes place through distinct mechanisms of micro-hydrodynamics and improved running-in behaviour respectively. Rodrigues *et al* [10] showed a reduced friction for elastohydrodynamic line contacts with surface textures imparted using a maskless electrochemical technique. The wear rate of the textured and untextured samples varied with respect to each other and was dependant on the degree of asperity interaction created by the contact load. Khaemba *et al* [11] showed the complex interaction of laser structured surfaces, friction and wear performance, with a particular focus on the surface textures interaction with surface active lubricant additives.

Surface texture features have been shown to provide a tribological advantage in a variety of tribological contacts when the geometric, loading and kinematic conditions are favourable. For reciprocating engine piston rings the greatest benefit for parasitic power loss appears when the texture features are at mid-stroke [6 and 7]. The apex seal's continuous unidirectional sliding in many ways emulate mid-stroke piston ring behaviour. An investigation of the potential benefit of laser surface texturing to reduce frictional losses in Wankel engine apex seals therefore is worthy of investigation.

This paper presents an investigation of the potential benefits of laser surface texturing to reduce frictional losses at the interface between Wankel engine apex seals and the epitrochoidal housing. To enable selection of a suitable set of texturing parameters from tribologically similar conjunctions in literature an analytical model of the seal dynamics is used to enable the tribological characterisation of the apex seal-housing conjunction. The texture features are applied to the seal working surface and then tested on an engine spin rig to determine if a reduction in frictional losses is achieved.

Experimental methodology

A Wankel engine spin rig has been created to ascertain the magnitude of parasitic frictional losses created, at the apex seal-housing interfaces. The test rig, which is shown in figure 1 is comprised of a 0.95 kW O.S. 49-PI Type II model rotary engine (1), electric motor (2), gear box (3) and a lever arm and load cell arrangement (4). The design of the chosen engine does not include side or corner seals. The only locations of contact between the rotor and the housing is at the rotors 3 apex seals and the side face of the rotor (figure 1(b)). During the tests the engine rotor is spun by the electric motor up to a speed of 8000 rpm, this is well within the engines operating range which extends from 7000 to 17,000 rpm. The friction reaction between the rotor and housing can be determined by measuring, via a load cell, the force restraining the engine housing from rotation (equilibrium). The reaction force results from the sum of the three apex seal-housing frictional forces. The friction force acting on each of the apex seals is shown in figure 1(b), an equal and opposite force on the housing would result.

The test rig is instrumented with thermocouples to measure the gas outlet temperature from the exhaust port and housing bulk metal temperature near to the location of the spark plug at 810°; the spark plug is removed for the current testing. The shaft speed is read by a dual beam Laser Doppler vibrometer.

The friction torque on the housing from the apex seals, T_F, can be determined from the experimental data from the summation of moments taken about the centre of the housing:

$$\sum M_0 = T_F + T_p + T_a + F_L X_1 + F_{pr} X_2 \quad (1)$$

Where, T_a is the mean torque created as result of friction at the shaft bearings and the rotor side face-housing interfaces. This value is determined experimentally by running the engine without the apex seals across the range of speeds investigated. F_L and X_1 are the measured reaction force of the load cell and the perpendicular distance of the reaction force to the housing centre respectively. F_{pr} and X_2 are the applied preload force and the perpendicular distance of the preload to the housing centre. Finally, T_p is the mean torque created due to the pressure variation within each of the chambers acting on the housing and can be determined by:

$$T_p = \frac{3}{6\pi} \sum_{\alpha=0}^{\alpha=6\pi} \sum_{\varphi=\alpha}^{\varphi=\alpha+2\pi} \left(\begin{bmatrix} r_x \\ r_y \end{bmatrix} \times \begin{bmatrix} PA_h \cos \varphi_n \\ PA_h \sin \varphi_n \end{bmatrix} \right) \quad (2)$$

Where, φ, describes the angular positions of the housing exposed to pressure of one chamber as it rotates through a full cycle. One full cycle of the rotor requires 3 rotations of the crank shaft $\left(\beta = \frac{\alpha}{3}\right)$. The pressure, P, in the chamber at any crank rotation position, α. A_h is the area of housing wall swept through during one degree crank rotation and φ_n is the direction normal to the area A_h. The components of the moment arm about the centre of housing are given as:

$$r_x = e \cos \alpha + \rho \cos \beta \quad (3)$$

$$r_y = e \sin \alpha + \rho \sin \beta \quad (4)$$

The average frictional power loss of the three apex seals is determined using the calculated contact kinematics and measured time average friction torque on the housing. In practice variations in frictional power loss occur within a single engine cycle due to fluctuations in entrainment speed, normal load and temperature, however, an approximation of the power loss assuming constant friction torque is given by:

$$P_F = \frac{3}{2\pi} \int_0^{2\pi} \mu_h W_h r\omega \cos(\vartheta) d\beta \approx \frac{T_F}{2\pi} \int_0^{2\pi} \frac{\bar{U}}{r} \cos(\vartheta) d\beta \quad (5)$$

Where the angle, ϑ, resolves the component of the friction force perpendicular to the moment arm created between the crank shaft centre and the apex seal-housing interface. The angle, ϑ, is defined by Handschuh and Owen [12] as:

$$\vartheta = \cos^{-1}\left(\frac{r^2 + \rho^2 + e^2}{2|r\rho|}\right) \quad (6)$$

Apex seal dynamics

An analysis of the kinematics and dynamics of the apex seal is conducted to ascertain the regime of lubrication of the apex seal-epitrochoidal housing interface. The normal contact load is critical to determine the regime of lubrication and texture features to ameliorate the frictional loss during this regime of lubrication. This analysis will allow a suitable texture analog to be selected from literature and to inform discussion of results.

The analysis considers a single apex seal in isolation, it is assumed that each of the three seals would experience the same conditions with a phase shift of $\frac{1}{3}$ of a cycle. The external forces which are considered to act on an apex seal in the current analysis are shown in figure 2. The forces considered on a single apex seal are as follows: the gas forces which act on the sides and back face of the seal, the spring force from the leaf spring and normal reaction forces with associated frictional components from the housing and rotor. The forces acting on the apex are resolved in both the radial and tangential directions. It is assumed the location of the seal can take one of binary set of positions at either edge of the rotor groove (figure 2). For the purpose of simplification the tilting degrees of freedom are ignored, further details of apex seal tilting behaviour are shown by Picard *et al* [13].

The contact forces between the apex seal-housing and apex seal-rotor interface can be determined using an inverse dynamics approach described by Handschuh and Owen [12]. In addition, a constant value is assumed for the coefficients of friction, in reality these would change as a function of speed, load and temperature. The equations of motion in matrix form can be written:

$$\begin{bmatrix} W_r \\ W_h \end{bmatrix} = \frac{1}{-1 - x\mu_h\mu_r} \begin{bmatrix} P_T A_T + ma_t - P_L A_L \\ P_b A_b - \frac{(P_T + P_L)}{2} A_b - ma_r + F_s \end{bmatrix} \begin{bmatrix} 1 & -x\mu_r \\ -\mu_h & -1 \end{bmatrix} \quad (7)$$

The equations are solved at each crank angle. A switching parameter is used in the model to allow for the apex seal to sit on either side of the groove. The criterion and the parameters which are affected by the change in location of the seal with respect to the rotor are given in equation (8). The parameter, x, is used to maintain the friction force between the rotor and seal in a constant direction as the current analysis does precludes the calculation of a slip velocity of the apex seal relative to the rotor.

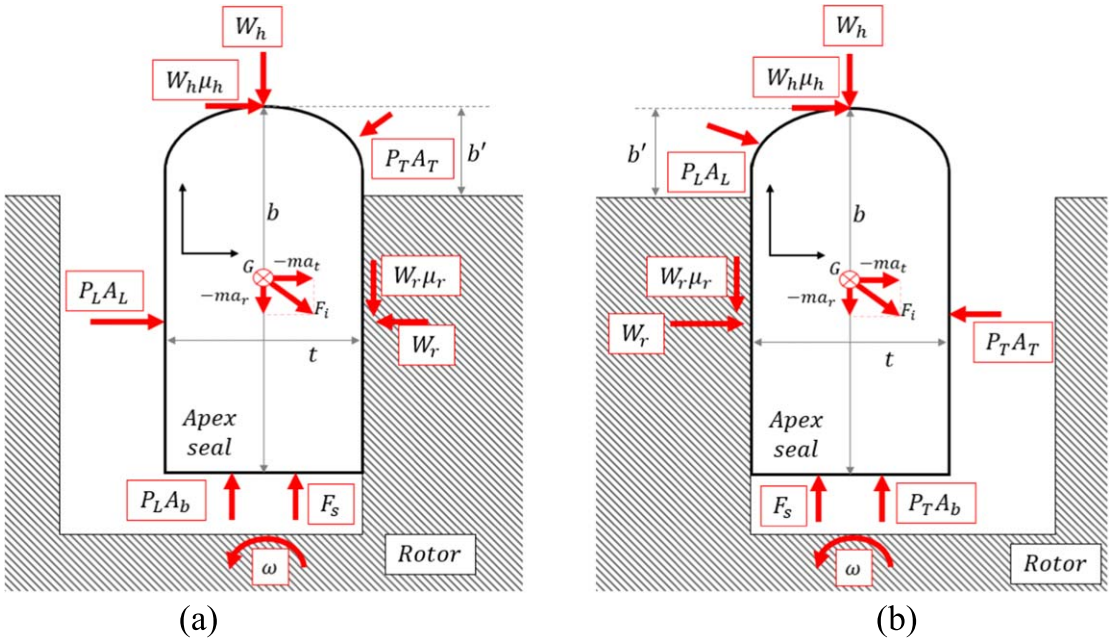

Figure 2. Diagram of forces on a radial lip seal in the two positions considered (a) at the trailing seal groove edge (b) at the leading seal groove edge.

$$\mathrm{W_r} > 0\begin{cases}\mathrm{A_L} = \mathrm{b'l}\\ \mathrm{A_T} = \mathrm{bl}\\ \mathrm{P_b} = \mathrm{P_T}\\ x = 1\end{cases} \quad \text{and} \quad \mathrm{W_r} < 0\begin{cases}\mathrm{A_L} = \mathrm{bl}\\ \mathrm{A_T} = \mathrm{b'l}\\ \mathrm{P_b} = \mathrm{P_L}\\ x = -1\end{cases} \tag{8}$$

The acceleration terms necessary to determine the inertial forces in equation (7) are given by Handschuh and Owen [12]:

$$\begin{bmatrix}\mathrm{a_r}\\ \mathrm{a_t}\end{bmatrix} = \begin{bmatrix}\cos\beta & \sin\beta\\ -\sin\beta & \cos\beta\end{bmatrix}\begin{bmatrix}-\omega_c^2\mathrm{e}\cos\alpha - \omega_r^2\rho\cos\beta\\ -\omega_c^2\,\mathrm{e}\sin\alpha - \omega_r^2\rho\sin\beta\end{bmatrix} \tag{9}$$

To be capable of predicting the tribological conditions at the apex seal-housing interface in the motored engine tests it is necessary to know the chamber pressure. It can be seen from the equations of motion (equation (7)) than the chamber pressures have an important role on the magnitude of contact forces. The volume of a chamber can be found during a cycle as [1]:

$$V = V_m + \frac{3\sqrt{3}}{2}e\rho l\left(1 - \sin\left(\frac{2}{3}\alpha + \frac{\pi}{6}\right)\right) \tag{10}$$

$$V_m = \left(\frac{\pi}{3}e + 2\rho\cos(\varphi_{\max}) + \left(\frac{2}{9}\frac{\rho^2}{e} + 4e\right)\varphi_{\max} - \frac{3\sqrt{3}}{2}\rho\right)le \tag{11}$$

The pressure in the engine chamber can either be measured or for a motored case the pressure in any chamber can be determined by considering the differential form of the first law of thermodynamics and equation of state for an ideal gas [14–16].

$$\dot{P} = \frac{R_g}{V}\left[\gamma(T_i\dot{m}_i - T\dot{m}_o) - P\dot{V}\left(\frac{1}{R_g} + \frac{1}{C_v}\right)\right] \tag{12}$$

$$\dot{T} = T\left(\frac{\dot{V}}{V} + \frac{\dot{P}}{P} + \frac{\dot{m}_o}{m} - \frac{\dot{m}_i}{m}\right) \tag{13}$$

Where T, P and m are the temperature, pressure and mass in the chamber respectively. While $\dot{\mathrm{m}}_\mathrm{i}$ is the mass flow rate into the chamber, $\mathrm{T_i}$ is the temperature of the air entering the chamber and $\dot{\mathrm{m}}_\mathrm{o}$ is the mass flow rate out of the chamber.

The mass flow rate through the exhaust port, inlet port, glow plug hole and general leakage can be approximated as flow through an orifice. The inequality shown in equation (14) is used to determine the condition of the flow from region 1 (upstream) to region 2 (downstream). The inequality is determined using the ratio of specific heats for air, γ. The exhaust port, intake port and glow plug are exposed sequentially while the chamber is constantly exposed to the general leakage area which is defined as 1.5 $\mathrm{mm^2}$ as suggested by Danieli *et al* [15] (it must be noted this area was for a different engine than that used in this study).

Table 1. Engine data used in analysis.

	0.95 kW engine fired	0.95 kW engine motored	28. 3kW engine fired	
P_α Maximum	2.5×10^6	2×10^6 (8000 rpm)	5×10^6	Nm^{-2}
e	3×10^{-3}		1×10^{-2}	m
k	7		6.5	–
m	7.8×10^{-4}		8.36×10^{-3}	kg
l	1.45×10^{-2}		5×10^{-2}	m
R	1×10^{-3}		1.25×10^{-3}	m
b	4.5×10^{-3}		9.5×10^{-3}	m
ω_r	$7800 \times \left(\frac{2\pi}{60}\right)$			$rad.s^{-1}$
η_0	1.4×10^{-3}			Pa.s at 150 C°
α	1×10^{-8}			$N^{-1} m^2$
E'	208×10^9			Nm^{-2}

$$\dot{m}_{\overrightarrow{12}} = C_d A \rho_1 \sqrt{\gamma R_g T_1} \begin{cases} \left(\frac{2}{\gamma+1}\right)^{\frac{\gamma+1}{2(\gamma-1)}}, & \frac{P_1}{P_2} > \left(\frac{\gamma+1}{2}\right)^{\frac{\gamma}{\gamma-1}} \\ \sqrt{\frac{2}{\gamma-1}\left[\left(\frac{P_2}{P_1}\right)^{\frac{2}{\gamma}} - \left(\frac{P_2}{P_1}\right)^{\frac{\gamma+1}{\gamma}}\right]}, & \frac{P_1}{P_2} \leqslant \left(\frac{\gamma+1}{2}\right)^{\frac{\gamma}{\gamma-1}} \end{cases} \tag{14}$$

Where C_d is the discharge coefficient, R_g is gas constant and ρ_1 is the density in the upstream region. The equations (12)–(14) are solved using a numerical Runge–Kutta approach with ODE-45.

Apex seal housing conjunction characterisation

To ascertain the most suitable form of surface textures to impart on the surface it is first necessary to use a lubrication chart to determine the regime of fluid film lubrication. The regime of fluid film lubrication can be determined from the non-dimensional groups presented by Winer and Cheng [17].

$$g_1 = \sqrt{\frac{\alpha^2 w^3}{\eta_0 \bar{U} R^2}} \tag{15}$$

$$g_3 = \sqrt{\frac{w^2}{\eta_0 \bar{U} E' R}} \tag{16}$$

Where w, η_0, α, are the load per unit length, lubricant dynamic viscosity and lubricant pressure viscosity coefficients respectively; E' and R are additionally the reduced elasticity and geometric parameters. The load per unit length is found from solving equation (7). The entrainment velocity $\bar{U}$ can be ideally determined from the tangential apex seal velocity as the housing is stationary [12]:

$$\bar{U} = \frac{1}{2}[(\omega_c e \cos\alpha + \omega_r \rho \cos\beta)\cos\beta - (\omega_c e \sin\alpha + \omega_r \rho \sin\beta)\sin\beta] \tag{17}$$

The lubrication regime for two different engines of varying size and power output are considered in this paper to show the tribological generality of the currently experimental set up to a range of Wankel engine geometries. The 0.95 kW engine on which the motored experimental analysis is conducted, in both fired conditions and during its motored condition (adiabatic compression). The result for the 28.3 kW (fired) engine is included to show the similarity in lubrication regime for Wankel rotary engines of varying size. The input conditions are shown in table 1.

The results in figures 3(a) and (b) show that the regime of lubrication for both engines during fired and motored conditions at 8000 rpm are in the piezo-viscous elastic regime. The grey regions indicate the transition between the four types of fluid film lubrication: piezoviscous rigid, piezoviscous elastic, isovicous elastic and isoviscous rigid. A range of points are plotted for each engine and cycle as the contact kinematics and load changes at each crank angle. The regime of lubrication remains almost entirely in piezo-viscous elastic for each engine across the whole cycle. Importantly the motored engine at higher speed tribological conjunctions mirror the fired engines in terms of elastic deflection and lubricant response.

The final aspect of the contact characterisation is to determine if a coherent fluid film is maintained between the contiguous surfaces. For such an analysis

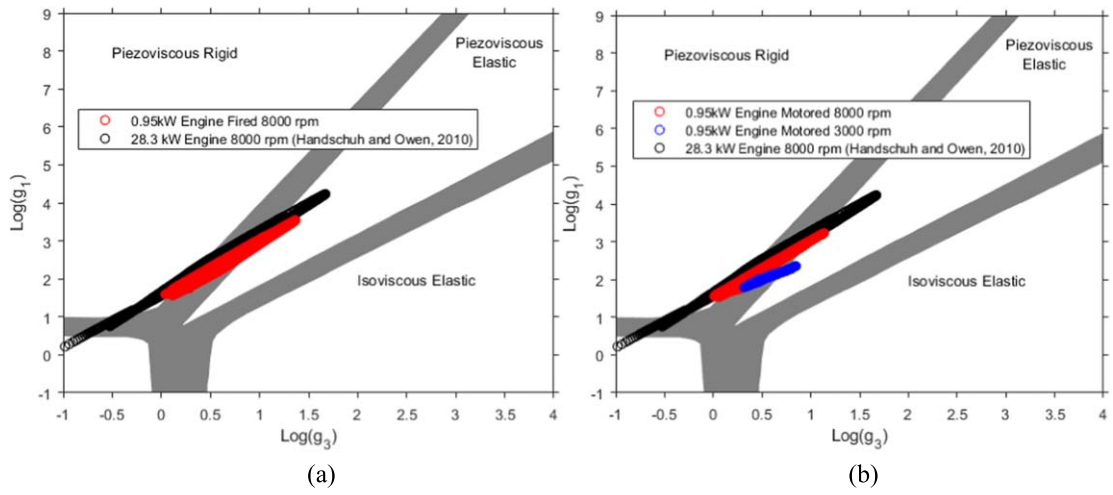

Figure 3. Lubrication regime of apex seals in various Wankel engines.

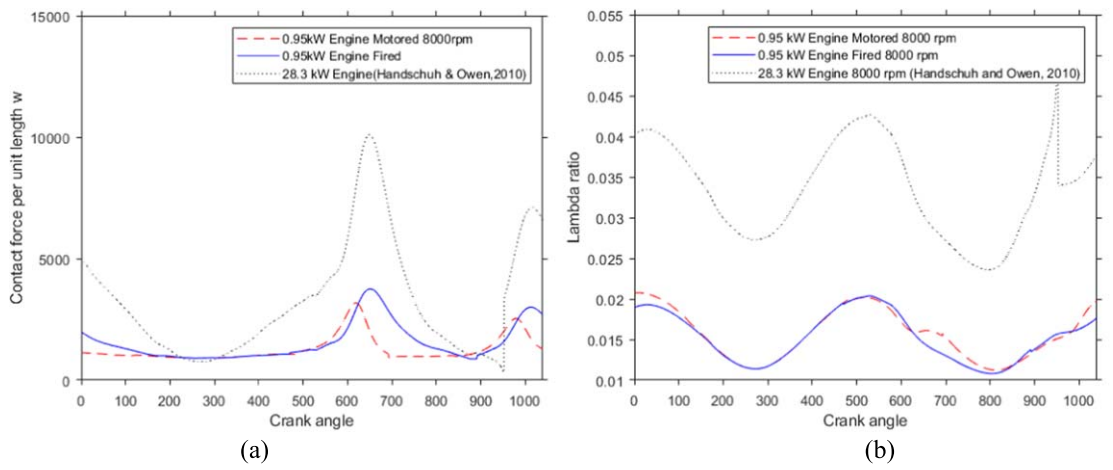

Figure 4. (a) Normal Contact force between housing and apex seal (b) Oil film ratio for housing apex seal conjunction.

the central film thickness equation for elastohydrodynamic conjunctions is used [18, 19]:

$$h = 2.922RG^{0.470}U^{0.692}W^{-0.166} \tag{18}$$

The severity of direct interaction of the contiguous surfaces is determined using the film thickness-surface roughness ratio parameter. The parameter can be written as [20]:

$$\lambda = h(\sigma_1^2 + \sigma_2^2)^{-0.5} \tag{19}$$

Figure 4(a) shows the calculated contact load on a single apex seal during one cycle. The pair of peaks results from compression and combustion in the chamber trailing and leading the seal which occur 360 crank angles apart. This occurs as it takes 3 full rotations of the crank to complete a full cycle of the rotor. In figure 4(b) the lubricant film to surface roughness ratio is shown. As the ratio is below 1, the contact is in a severe mixed/boundary regime of lubrication.

The analysis conducted in this section has shown that for 0.95 kW and a 28.3kW engine the apex seal house conjunction operates in a mixed elastohydrodynamic regime of lubrication. This finding will be used in the following section to select laser surface texture parameters from analog conjunctions which have been shown to be successful in reducing friction in open literature.

Laser surface texturing

The lubrication regime analysis demonstrates the contact falls within a piezo-viscous elastic regime of lubrication - otherwise known as elastohydrodynamic lubrication, with a rectangular contact footprint (line contact). The film thickness prediction indicates a partial break down of the lubricating film will occur and as a result, interaction of the contiguous surfaces.

A survey of recent literature was conducted to find effective texture geometries for analogous mixed elastohydrodynamic line contacts with comparable entrainment velocities. It was found the conditions presented in the combined experimental and experimental analysis

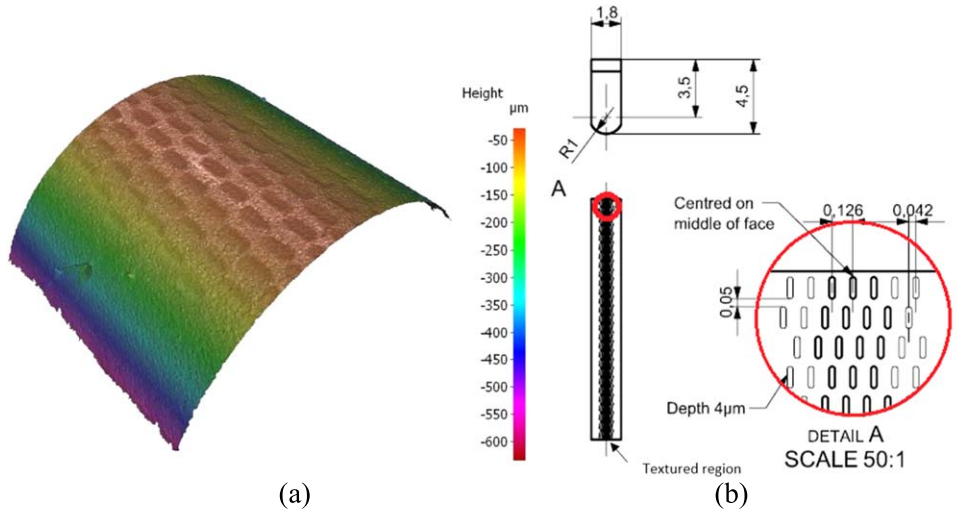

Figure 5. Laser surface textured seal surface.

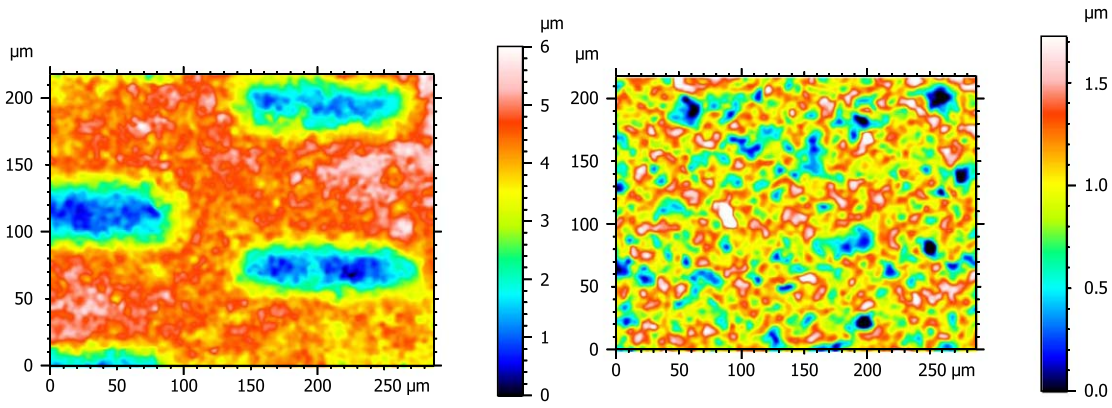

Figure 6. (a) Textured surface and (b) surface roughness of seal working surface before testing.

of Marian *et al* [21] corresponded well to many of the aforementioned aspects. The texture features described in figure 5 are largely based on those described by of Marian *et al* [21]. The texture width of 45 micro metres was selected as the lower limit of the capability of the laser (due to the spot size). This width was minimised to not be significantly larger than the expected Hertzian contact width for the smaller capacity engine used in this study (a suggested design parameter from Marian *et al* [21]).

The laser surface texture features are applied to the curved surface of the apex seal which seals the combustion chamber by pressing against the housing surface as shown in figure 1 and described in table 2. The texture features are applied across the crown of the apex seal using a 20 W average power, 5 axis machine with fibre laser by amplitude source. The pulse energy and wavelength are 40 μJ and 1030 nm respectively. Topographic characterisation of the seal surface was conducted after texturing using an Alicona focus variation microscope to confirm conformance to the specified surface design with respect to form and surface roughness (figure 5).

Table 2. Surface texture parameters.

Parameter	Value	Unit
Texture depth	4	μm
Length (perpendicular to sliding direction)	130	μm
Width (direction of sliding)	45	μm
Centre distance (sliding direction)	0.42	μm
Centre distance (perpendicular to sliding direction)	90	μm

The textured surface was measured using focus variation microscopy with a x50 objective. Filtering the height data by form removal using a second degree polynomial the surface texture features can be clearly shown in figure 6(a). In figure 6(b) a section of the untextured seal surface roughness is isolated using a Gaussian (ISO 16610-61) filter with 80 μm cut-off in addition to the form removal. The specific waviness and roughness values are presented for new and worn surfaces in the results section. Surface height maps of the textured surface and the surface roughness of seal before testing are shown in figure 6.

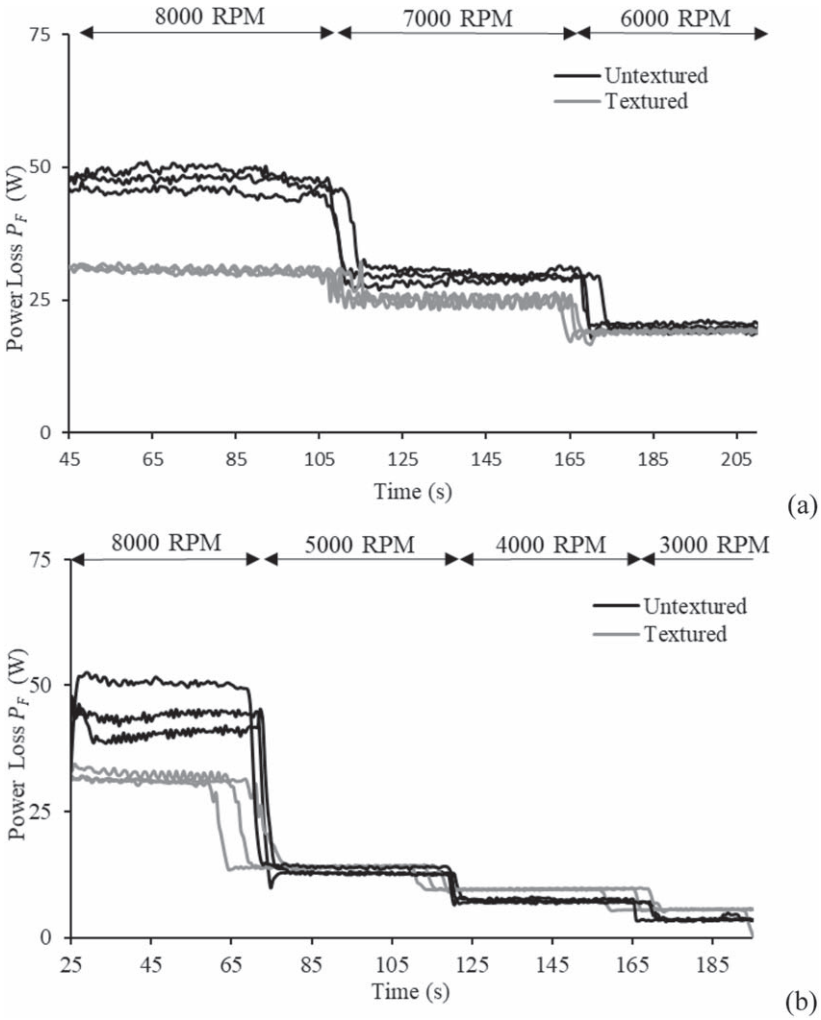

Figure 7. Power loss (a) between 8000 and 6000 rpm and (b) 5000 and 3000 rpm.

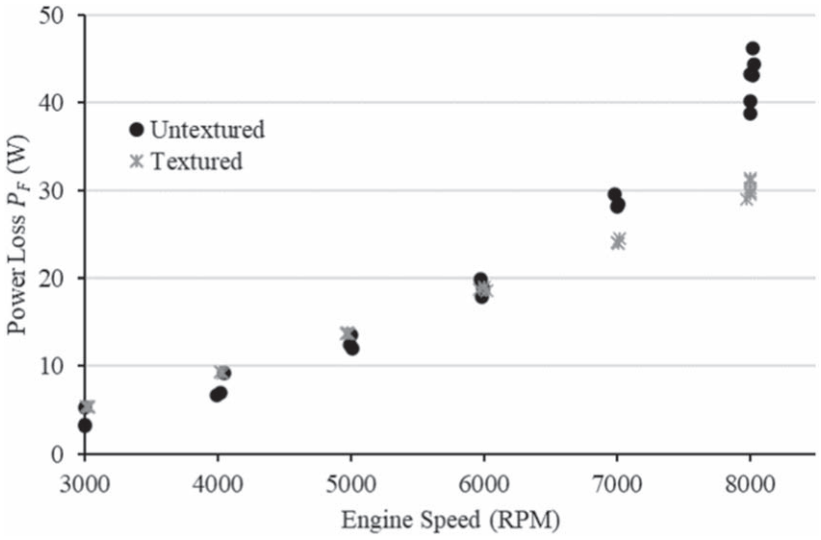

Figure 8. Average power loss with motored engine speed.

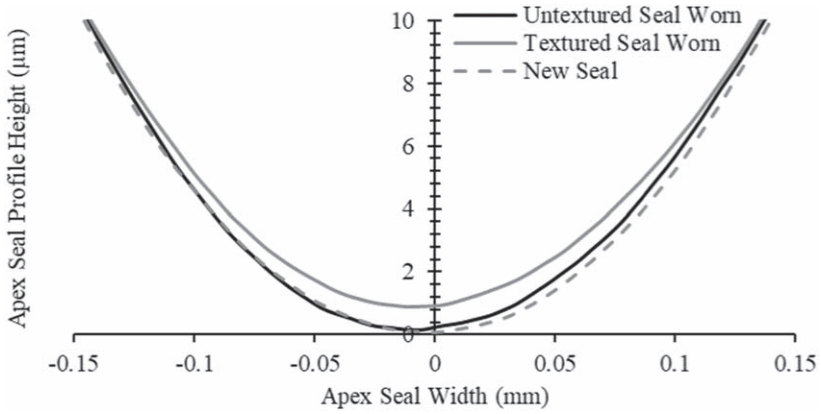

Figure 9. Variation of calculated contact force, entrainment speed and central film thickness.

Results

The test protocol was created to minimise the time duration of the experiments from the initial condition (8000 rpm) at which the housing temperature was allowed to reach thermal equilibrium. The aim of this was to reduce temperature changes which can significantly alter bulk lubricant viscosity. The speed range between 8000 and 3000 rpm was covered with two tests, each repeated 3 times, for each set of seals. During the first test the engine was allowed to reach thermal equilibrium at 8000 rpm before reducing the engine speed to 7000 rpm and then 6000 rpm (each for 30 s). The second test again consisted of attaining thermal equilibrium of the motored engine at 8000 rpm although this time the engine speed was reduced to 5000, 4000 and then 3000 rpm; each for a period of 30 s. An automotive 0W-40 lubricant was fed to engine using the carburettor. The air intake was set to wide open throttle for all runs, drawing in air at room temperature.

The results for the textured and untextured seals are shown in figure 7. The data shows the measured friction power loss of all three apex seals for a number of repeated measurements. The engine test procedure consisted of an initial period where the engine was spun at a constant speed of 8000 rpm until the housing temperature stabilised, at which point the recordings shown in figures 7(a) or (b) were made. In figures 7(a) and (b) the engine rotational speeds were maintained at 8000, 7000 and 6000 rpm and 8000, 5000, 4000 and 3000 rpm respectively.

The average power loss for each operation speed is shown in figure 7. The results show a reduction in parasitic power loss can be achieved through the application of texture features during the higher range of operating speeds investigated. The texture features however marginally increase losses at the lower rotational (relative sliding) speeds. Similar findings have been shown for piston compression rings in reciprocating engines, in which textures produced improve load capacity at mid-stroke (high entrainment speed) while a breakdown of lubricating fluid film at reversal (low entrainment) is observed [7, 8]. Indeed, the Marian *et al* [21] textures for the analogous EHL line contact which were the basis of design used in this work also show best performance (reduction in friction) at high entrainment speeds.

To determine the physical mechanism by which the textured surface achieves a reduction in friction the seal surfaces were measured to determine any change in surface form, waviness and roughness. The surface form of the seals was measured using a focus variation microscope with x20 objective providing a field of view of 720 $\times$ 540 μm. The result shown in figure 9 are each comprised of 9 measurements on each set of seals (3 on each seal). The mean surface form of each measurement is calculated by extracting ~1624 profiles in the direction of sliding. The mean surfaces from each measurement are aligned so that the area which experiences little contact and very low wear align. These regions can be observed in the vicinity of $\pm$0.15 mm in figure 9. The results for the new and worn seals (with and without texturing) are shown in figure 9.

The results in figure 9 show that the textured seal experiences significantly more wear during the experiments than the untextured seal. An increase in wear rate for counter formal textured surfaces and a corresponding decrease in friction has also been reported by Kovalchenko *et al* [9]. The worn surface form has an increased radius in comparison to the new seal (1.03 mm to 1.11 mm). Equation (16) shows the film thickness dependency on the effective radius ($h \propto R^{0.69}$) and therefore the improved comfortability of the worn seal would increase the surface separation. During the severe mixed and boundary regime of lubrication small increases of surface separation can significantly reduce frictional loss [22].

As well as the mean separation, the surface roughness also has a significant role in mixed and boundary regime frictional behaviour. Figure 10 shows the surface height maps of the surface roughness of the textured (a) and untextured (b) seal surfaces after

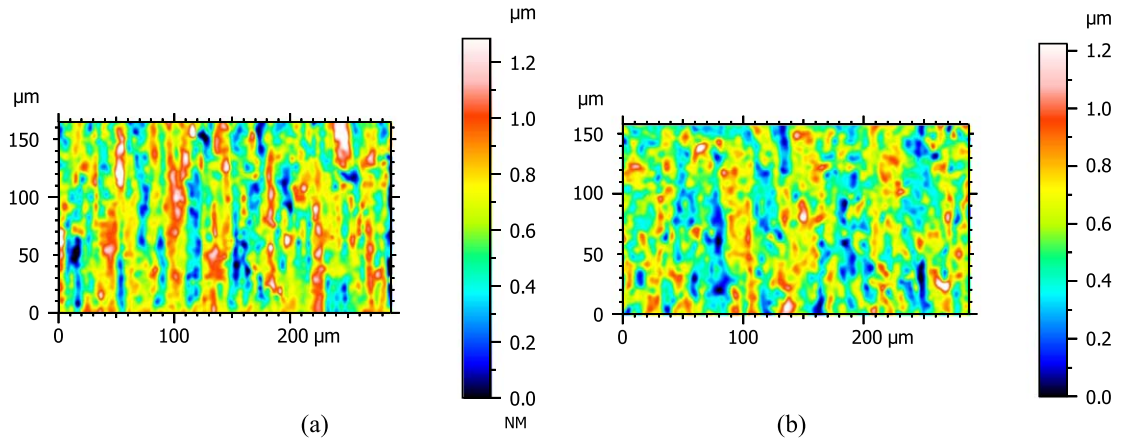

Figure 10. (a) Textured seal roughness and (b) untextured seal surface roughness.

Table 3. Surface topography components (± SD).

Parameter	New seal	Worn textured seal	Worn untextured seal	Unit
R_a (in direction of sliding)	0.18 ± 0.02	0.10 ± 0.02	0.09 ± 0.01	μm
R_q (in direction of sliding)	0.23 ± 0.03	0.12 ± 0.02	0.11 ± 0.02	μm
S_a (of surface waviness)	0.07 ± 0.02	0.18 ± 0.03	0.13 ± 0.03	μm

running. Surface roughness measurements are conducted using a focus variation method with x50 objective. The surface form and waviness are removed, as described previously. In comparison to the isotropic surface roughness of the new seal (figure 6(b)), the worn surfaces in figure 10 show striated surface features in direction of sliding (north-south direction) due to surface abrasion.

The arithmetic mean deviation and root mean square of the surface heights taken in the direction of sliding are shown in table 3. The values of these are obtained from 9 measurements on each set of seals (3 on each seal). From each measurement area (see figure 10 for one example) ~1624 profiles in the direction of sliding were extracted. The roughness (R_a and R_q) of both the textured and untextured worn surfaces are very similar. The surface roughness is therefore not thought to cause the difference in frictional behaviour. Both surfaces show a reduction in roughness amplitude due to surface polishing. It was not possible to distinguish deterministic texture features on the worn surface after the tests. To determine if the texture features had altered the surface topography the areal arithmetic mean deviation of the surface waviness which had been filtered from the surface measurement shown in figure 10 is displayed in table 3.

The areal arithmetic mean deviation of the surface waviness is also shown in table 3. The waviness filtered using a using a Gaussian (ISO 16610-61) filter with 80 μm cut-off shows an increase in amplitude for the textured seal. An increased waviness of the moving surface has been shown by Venner and Lubrecht [23] to produce enhanced lubricant entrainment and average film thickness during pure sliding. This provides an explanation for a secondary mechanism in addition to the improved surface conformability previously discussed through which the friction reduction was attained. To confirm both of these mechanisms a transient analysis of the elastohydrodynamic problem is necessary.

Conclusion

This paper characterises for both motored and fired rotary Wankel engines, tribological conditions at the apex seal-housing conjunction. The contact is found to reside in the mixed elastohydrodynamic regime of lubrication, and is therefore suitable for improvement through applied texture features from analogous line contacts; the contacts are modified on one surface via laser processing on the apex seals face. The experimental results show laser surface texture features suitable for elastohydrodynamic line contacts can reduce frictional power loss up to 30% at the higher speeds tested (8000 rpm). The paper shows that laser surface texture features are a potential way of reducing parasitic power loss in Wankel rotary engines. The mechanism for the friction reduction is a change in surface form of the textured and untextured surfaces resulting from changed wear behaviour of the textured surface. The current paper only evaluates a single set of surface texturing parameters and therefore there is significant scope for optimisation of surface texture parameter for the conjunction under investigation in future work.

Acknowledgments

The authors would like to thank the Manufacturing Technology Centre (MTC) for fabricating the surface texture features on the seal surface.

ORCID iDs

Nick Morris https://orcid.org/0000-0001-9463-647X

References

[1] Yamamoto K 1981 *Rotary Engine* (Tokyo, Japan: Sankaido) ISBN-10: 9997341171
[2] Zhang S, Liu J and Zhou Y 2019 Effect of DLC coating on the friction power loss between apex seal and housing in small Wankel rotary engine *Tribol. Int.* **134** 365–71
[3] Umer J, Morris N, Leighton M, Rahmani R, Howell-Smith S, Wild R and Rahnejat H 2018 Asperity level tribological investigation of automotive bore material and coatings *Tribol. Int.* **117** 131–40
[4] Etsion I 2005 State of the art in laser surface texturing *J. Trib.* **127** 248–53
[5] Etsion I and Sher E 2009 Improving fuel efficiency with laser surface textured piston rings *Tribol. Int.* **42** 542–7
[6] Ryk G, Kligerman Y and Etsion I 2002 Experimental investigation of laser surface texturing for reciprocating automotive components *Tribol. Trans.* **45** 444–9
[7] Vladescu S C, Olver A V, Pegg I G and Reddyhoff T 2015 The effects of surface texture in reciprocating contacts—an experimental study *Tribol. Int.* **82** 28–42
[8] Morris N, Rahmani R, Rahnejat H, King P D and Howell-Smith S 2016 A numerical model to study the role of surface textures at top dead center reversal in the piston ring to cylinder liner contact *J. Tribol.* **138** TRIB-15-1087
[9] Kovalchenko A M, Erdemir A, Ajayi O O and Etsion I 2017 Tribological behavior of oil-lubricated laser textured steel surfaces in conformal flat and non-conformal contacts *Materials Performance and Characterization* **6** 1–23
[10] Rodrigues T A, Arencibia R V, Costa H and da Silva W M Jr 2020 Roughness analysis of electrochemically textured surfaces: effects on friction and wear of lubricated contacts *Surface Topography: Metrology and Properties* 024011
[11] Khaemba D N, Azam A, See T, Neville A and Salehi F M 2020 Understanding the role of surface textures in improving the performance of boundary additives: I. Experimental *Tribol. Int.* **146** 106243
[12] Handschuh R F and Owen A K 2010 Analysis of apex seal friction power loss in rotary engines. NASA Glenn Research Center; Cleveland, OH, NASA Technical Memorandum No. 2010-216353
[13] Picard M 2014 *Development of Multiscale Models for the Performance of the Gas and Oil Seals in Rotary Engines* (Cambridge, Massachusetts: Massachusetts Institute of Technology)
[14] Sierens R, Baert R, Winterbone D E and Baruah P C 1983 A comprehensive study of Wankel engine performance (No. 830332) *SAE Technical Paper* (https://doi.org/10.4271/830332)
[15] Danieli G A, Ferguson C R, Heywood J B and Keck J C 1974 Predicting the emissions and performance characteristics of a Wankel engine *SAE Trans.* pp 805–20
[16] Danieli G A, Keck J C and Heywood J B 1978 Experimental and theoretical analysis of wankel engine performance (No. 780416) *SAE Technical Paper* (https://doi.org/10.4271/780416)
[17] Winer W O and Cheng H S 1980 Film thickness, contact stress and surface temperatures *Wear Control Handbook* pp 81–141 ASME New York, ISBN0317336401, 9780317336405
[18] Dowson D, Higginson G R and Whitaker A V 1962 Elasto-hydrodynamic lubrication: a survey of isothermal solutions *J. Mech. Eng. Sci.* **4** 121–6
[19] Pan P and Hamrock B J 1989 Simple formulas for performance parameters used in elastohydrodynamically lubricated line contacts *ASME. J. Tribol.* **111** 246–51
[20] Tallian T E 1967 On competing failure modes in rolling contact *ASLE Trans.* **10** 418–39
[21] Marian M, Tremmel S and Wartzack S 2018 Microtextured surfaces in higher loaded rolling-sliding EHL line-contacts *Tribol. Int.* **127** 420–32
[22] Stribeck R Die wesentlischen Eigenschaften der Gleit- und Rollenlager. Zeitschrift des Vereines deutscher Ingenieure 1902; 46(37):1341-1348 (pt I) & 46(38):1432-1438 (pt II) & 46(39) 1463-1470 (pt III)
[23] Venner C H and Lubrecht A A 1994 Transient analysis of surface features in an EHL line contact in the case of sliding *Journal of Tribology-Transactions of the ASME* **116** 186–93